Roughness Implementation in FENSAP-ICE: Model Calibration and Influence on Ice Shapes

Héloïse Beaugendre,* François Morency,† and Wagdi G. Habashi‡
McGill University, Montreal, Quebec H3A 2S6, Canada
and
Pascal Benquet§
Newmerical Technologies International, Montreal, Quebec H3A 2M7, Canada

Downloaded by PRINCETON UNIVERSITY on August 28, 2015 | http://arc.aiaa.org | DOI: 10.2514/2.7214

Introduction

NOT all in-flight icing certification conditions can be wind/ice-tunnel tested, flight tested, tanker tested, or encountered in natural icing testing. Numerical simulation, thus, complements such tests and allows the safe exploration of the complete combined flight/icing envelopes. As such, two-dimensional and quasi-three-dimensional in-flight ice accretion simulation codes have been in use by the aerospace industry as an aid to the certification process. Numerically predicted ice shapes are manufactured from a light material and attached as disposable profiles on an aircraft, to investigate it for stability and control under model icing encounters. Although efficient for calculating ice shapes on simple geometries, these first-generation simulation codes have limitations for complex truly three-dimensional geometries. Current advanced computational fluid dynamics (CFD) technologies are quickly overcoming these limitations.

To predict ice accretion, accurate convective heat fluxes on smooth and rough surfaces are needed. In most current icing codes, convective heat fluxes are computed by solving integral boundary-layer equations and using an equivalent sand grain parameter to account for the roughness of the iced surface. The finite element Navier–Stokes analysis package for ice (FENSAP-ICE) is a new three-dimensional CFD-based in-flight icing simulation system, built in a modular and interlinked way to successively solve each of flow, impingement, accretion, heat loads, and performance degradation. The code models the flow based on the Euler/Navier–Stokes equations for the clean and degraded flow and on new partial differential equations (PDEs) for each of the other three icing processes: The collection efficiency is solved with the DROP3D[1] module, a one-shot Eulerian method (as opposed to traditional particle-by-particle Lagrangian techniques), and ice accretion shapes are computed with ICE3D,[2] a finite volume method (as opposed to one-dimensional control volume approaches). After much investigation of the most appropriate turbulence model for icing situations, the Spalart–Allmaras[3] (S–A) one-equation model was selected for its simplicity and for the ease of implementation of roughness calculations. In this Technical Note, we first present the roughness calibration results for the model and then show the strong influence of such roughness on ice shape predictions.

Presented as Paper 2003-1222 at the 41st Aerospace Sciences Meeting and Exhibit, Reno, NV, 6 January 2003; received 12 May 2003; revision received 28 July 2003; accepted for publication 28 July 2003. Copyright © 2003 by the authors. Published by the American Institute of Aeronautics and Astronautics, Inc., with permission. Copies of this paper may be made for personal or internal use, on condition that the copier pay the $10.00 per-copy fee to the Copyright Clearance Center, Inc., 222 Rosewood Drive, Danvers, MA 01923; include the code 0021-8669/03 $10.00 in correspondence with the CCC.

*Research Associate, Computation Fluid Dynamics Laboratory, 688 Sherbrooke Street West.

†Research Associate, Computation Fluid Dynamics Laboratory, 688 Sherbrooke Street West.

‡Professor and Director, Computation Fluid Dynamics Laboratory, 688 Sherbrooke Street West. Associate Fellow AIAA.

§Aerodynamicist, NTI, 680 Sherbrooke Street West.

Roughness Model Calibration Within FENSAP

A good prediction of heat fluxes, hence, accurate turbulence and roughness modeling, is essential to a credible simulation of ice accretion. FENSAP-ICE's current airflow module, FENSAP, has a one-equation turbulence model (S–A), as well as two-equation models (low Reynolds and high Reynolds k–ε and k–ω). Let us describe the ice roughness calibration using the S–A model, for which, the transport equation for the dimensionless turbulent viscosity $\tilde{\nu}$ is:

$$\frac{\partial \tilde{\nu}}{\partial t} + u_j \frac{\partial \tilde{\nu}}{\partial x_j} = \frac{1}{\sigma Re_\infty} \frac{\partial}{\partial x_k}\left[(\nu + \tilde{\nu})\frac{\partial \tilde{\nu}}{\partial x_k}\right] + c_{b1}(1 - f_{t2})\tilde{S}\tilde{\nu} - \left[c_{w1} f_w - \frac{c_{b1}}{\kappa^2} f_{t2}\right]\frac{1}{Re_\infty}\left(\frac{\tilde{\nu}}{d}\right)^2 + \frac{c_{b2}}{\sigma Re_\infty}\frac{\partial \tilde{\nu}}{\partial x_k}\frac{\partial \tilde{\nu}}{\partial x_k} + Re_\infty\left(f_{t1}\Delta U^2\right) \tag{1}$$

where d is the distance from the wall, $\tilde{S}$ is the modified vorticity where $\tilde{S} = S(1/Re_\infty)(\tilde{\nu}/\kappa^2 d^2) f_{v2}$, with S the vorticity, c_{b1}, c_{b2}, c_{w1}, κ, and σ are the closure coefficients, and f_w and f_{v1} are the closure functions. The tripping functions, f_{t1} and f_{t2}, permit user control to trigger transition from laminar to turbulent flow. This model has been shown to be particularly attractive for unstructured meshes. Spatial discretization is carried out by a finite element method (FEM), and the equation is linearized by a Newton method. A new artificial viscosity method[4] (ISOD) based on diffusion along isovalues surfaces is used to prevent numerical oscillations. To advance the solution in time, an implicit Gear scheme is used, along with a generalised mininmal residual procedure to solve iteratively the resulting matrix system. Heat fluxes at the wall are accurately calculated via a consistent FEM approach.[5]

The extension for rough-wall treatment,[6] essential for icing simulation, has been included in the model. For a roughness coefficient k_s (the conventional Nikuradse sand grain roughness) the distance from the wall is increased, as follows, relative to the min distance $d_{\min}$:

$$d = d_{\min} + 0.03 k_s \tag{2}$$

This extension requires nonzero wall values of $\tilde{\nu}$ and, thus, of ν_T and a mixed (or Robin) wall boundary condition $\partial\tilde{\nu}/\partial n = \tilde{\nu}/d$.

The logarithmic velocity profile of a boundary layer upon a rough surface has the form[7]

$$u^* = (1/\kappa)\,\ln y^* + B - \Delta B$$

with the constants defined by $\kappa = 0.41$ and $B = 5$. The correction added to the constant B and ΔB is related to the roughness coefficient by the following formula:

$$\Delta B = (1/\kappa)\,\ln k_s^* - 3.65$$

with $k_s^* = u_s k_s/\nu$.

The logarithmic velocity profile can then be directly related to the roughness coefficient by

$$u^* = (1/\kappa)\,\ln(y/k_s) + 8.5 \tag{3}$$

The agreement between the computed velocity profiles and the Nikuradse universal profiles in the log layer, Eq. (3), is demonstrated in Ref. 8. Mills and Hang (see Ref. 7) have deduced a semi-empirical formula for the skin-friction coefficient on a sand-roughened flat-plate:

$$c_f = [3.476 + 0.707\,\ln(x/k_s)]^{-2.46} \tag{4}$$

The computed c_f curves are compared with Eq. (4) in Fig. 1a, and it can be seen that the S–A model gives results that are quite close to the formula. In Fig. 1b, the experiments performed by Blanchard[9] are compared to FENSAP S–A, as well as to the ONERA[10] and The Boeing Company results. In the experiments, the surface is covered with hemispheres with a spacing of four times their height. For an external velocity of 58 m/s, the reduced equivalent sand grain roughness k_s^* is about 50. In this case, the Stanton number is fairly well

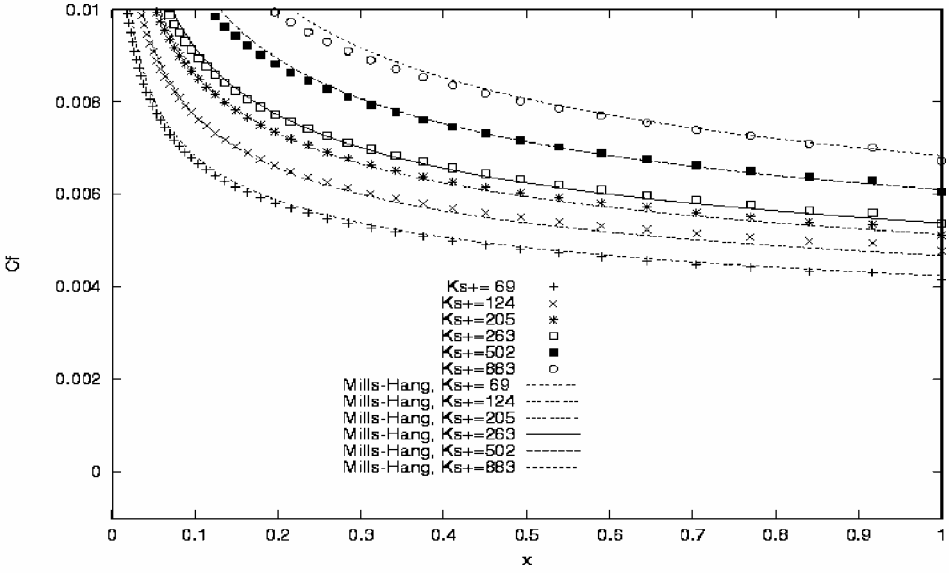

Fig. 1a Skin-friction coefficient for fully rough plates obtained with S–A compared with Eq. (4).

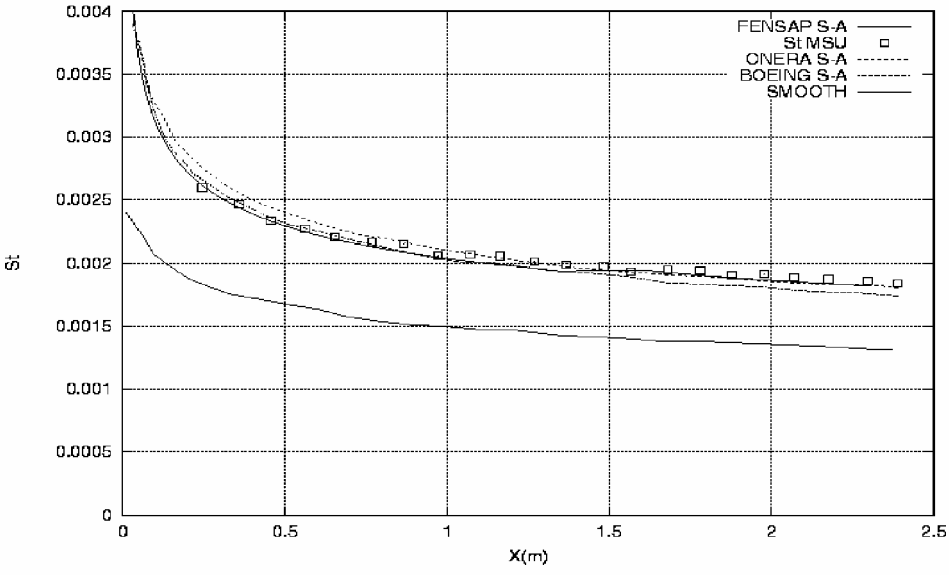

Fig. 1b Stanton number predictions, MSU experiment (58 m/s): comparison between S–A ONERA, S–A Boeing, and S–A FENSAP.

reproducedby the S–A model in the three codes. The velocity profile for a pipe flow obtained with FENSAP using S–A for a smooth and for several rough pipe walls have been compared[8] with measurements and demonstrate good agreement with the experimental data.

Influence of Roughness on Ice Shapes

As demonstrated in the preceding section, roughness will affect skin friction, heat transfer rates, and the transition point from laminar to turbulent flow. Changing the roughness parameter will modify the convective heat transfer rate and influence the growth rate, the shape, and even the type of ice (rime or glaze). When the sand grain roughness is increased, the convective heat transfer will also increase, freezing all droplets on impact and producing rime ice (Fig. 2), whereas a lower convective heat transfer will lead to only a fraction of the droplets freezing on impact and produce glaze ice (Fig. 2). Therefore, ice shapes are quite sensitive to roughness sizes.

Empirical correlations can be found in the literature to evaluate the effect of roughness, but these correlations exist only for well-defined types of roughness elements and are not directly relevant to ice accretion calculations. In icing, the roughness sizes can vary with the ambient icing conditions, the location on the surface, and the accretion time. The influence of these parameters on roughness is complex and remains an active research field, with computational icing codes facing the problem of determining the most appropriate sand grain roughness for given icing conditions. An empirical correlation relating the surface roughness equivalent sand grain parameter has been developed for LEWICE, Eq. (5), and this correlation is also used inside FENSAP-ICE:

$$k_s = \left[\frac{k_s/C}{k_s/C)_{\text{base}}}\right]_{V_\infty} \left[\frac{k_s/C}{k_s/C)_{\text{base}}}\right]_{\text{LWC}} \left[\frac{k_s/C}{k_s/C)_{\text{base}}}\right]_{T_s} k_s/C)_{\text{base}} \tag{5}$$

with

$$\left[\frac{k_s/C}{k_s/C)_{\text{base}}}\right]_{V_\infty} = 0.4286 + 0.00444139V_\infty$$

$$\left[\frac{k_s/C}{k_s/C)_{\text{base}}}\right]_{\text{LWC}} = 0.5714 + 0.2457(\text{LWC}) + 1.2571(\text{LWC})^2$$

$$\left[\frac{k_s/C}{k_s/C)_{\text{base}}}\right]_{T_s} = 46.8384\left(\frac{T_s}{1000}\right) - 11.2037$$

$$\left.\frac{k_s}{C}\right)_{\text{base}} = 0.00117$$

Downloaded by PRINCETON UNIVERSITY on August 28, 2015 | http://arc.aiaa.org | DOI: 10.2514/2.7214

Downloaded by PRINCETON UNIVERSITY on August 28, 2015 | http://arc.aiaa.org | DOI: 10.2514/2.7214

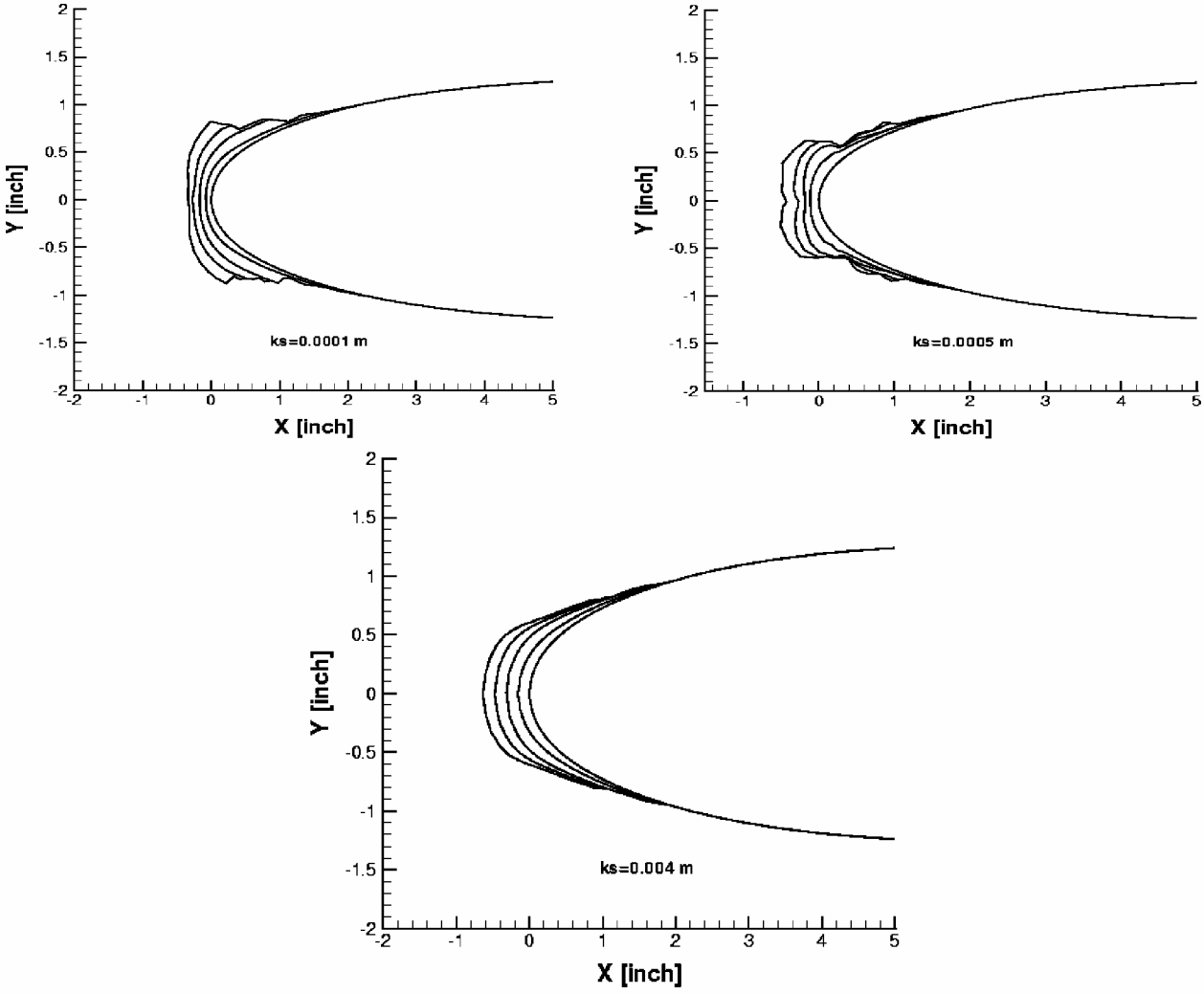

Fig. 2 Effect of roughness on a NACA 0012 wing, the ambient icing conditions are the following: angle of attack = 0 deg, $T_\infty = -14°$C, $U_\infty = 93.88$ m/s, $d = 30.7$ μm, LWC = 0.94 g/m^3, and $t = 225$ s of ice accretion.

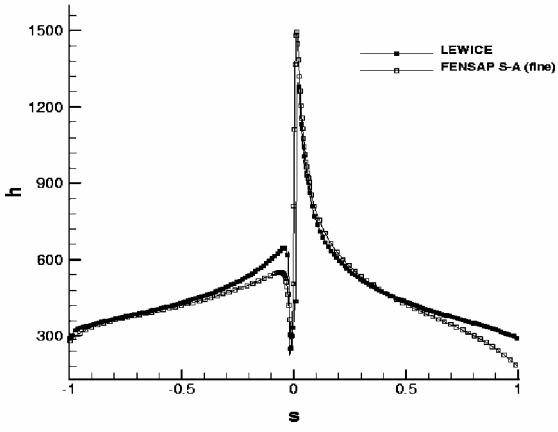

Fig. 3a Convective heat transfer coefficient (watts per square meter degrees Kelvin) distribution against the distance from stagnation point, comparison between FENSAP S-A and LEWICE solution.

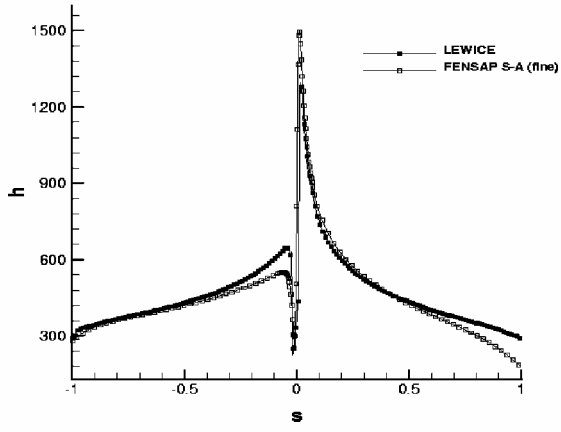

Fig. 3b Run 403 from LEWICE CD-ROM[11] with ambient icing conditions of angle of attack = 4 deg, $T_\infty = 262.04$ K, $U_\infty = 102.8$ m/s, $d = 20$ μm, and LWC = 0.55 g/m^3.

In all equations, the velocity is in meters per second, the liquid water content (LWC) in grams per cubic meter, and the static temperature is in degrees Kelvin.

An evaluation of our approach, consisting in solving the Navier–Stokes equations along with the one-equation turbulence model S–A and the equivalent roughness parameter of LEWICE, has been performed on a NACA 0012 wing. The ambient conditions selected for this test case correspond to LEWICE run 403 (Ref. 11), and the equivalent sand grain roughness parameter in both approaches is set at 0.55 mm. LEWICE uses an integral method to solve the boundary-layer equations. LEWICE and FENSAP S–A convective heat flux coefficients are compared in Fig. 3a. The differences between the two curves close to the trailing edge are most probably due to the thickness of the boundary layer that is not taken into account by LEWICE. Close to transition points, the differences are most probably induced by the roughness coefficient that is well

calibrated for LEWICE but does not play an identical role in the S–A model as in an integral method. However, although the two approaches are quite different, their solutions agree pretty much, and the results are satisfactory. In this test case, on the clean airfoil, the impingement solution of DROP3D and ICE3D are identical (Ref. 8). In Fig. 3b, the LEWICE numerical solution obtained after 1 min of accretion is compared to the ICE3D solution, and they agree pretty well. The small differences between the convective heat flux coefficients of LEWICE and FENSAP S–A do not significantly influence the ice shape and, thus, confirm the validity of our convective heat fluxes and validate our PDE-based icing approach.

Conclusions

The one-equation S–A turbulence model has been implemented in the three-dimensional FEM flow solver, FENSAP, of the FENSAP-ICE in-flight icing simulation system. The surface roughness of iced surfaces has been taken into account with an equivalent sand grain roughness parameter. The effects of roughness on the flow solution have been successfully validated against numerical and experimental results, and the roughness effects on ice shapes have been demonstrated through a NACA 0012 wing test case. The S–A model has proven to be robust, to be easy to use, and showed good agreement with theory and experiments, making it a valuable tool for PDE-based in-flight icing simulations.

Acknowledgment

We would like to thank Philippe Spalart of The Boeing Company for his advice in implementing the roughness within his turbulence model.

References

[1]Bourgault, Y., Habashi, W. G., Dompierre, J., and Baruzzi, G. S., "A Finite Element Method Study of Eulerian Droplets Impingement Models," *International Journal for Numerical Methods in Fluids*, Vol. 29, 1999, pp. 429–449.

[2]Beaugendre, H., Morency, F., and Habashi, W. G., "ICE3D, FENSAP-ICE's In-flight Ice Accretion Module," *Proceedings of the 48th CASI Annual Conference*, Canadian Aeronautics and Space Inst., Toronto, 2001, pp. 271–276.

[3]Spalart, P. R., and Allmaras, S. R., "A One-Equation Turbulence Model for Aerodynamic Flows," AIAA Paper 92-0439, Jan. 1992.

[4]Remaki, L., Beaugendre, H., and Habashi, W. G., "ISOD—An Anisotropic Isovalue-Oriented Diffusion Artificial Viscosity for the Euler and Navier-Stokes Equations," *Journal of Computational Physics*, Vol. 186, No. 1, 2003, pp. 279–294.

[5]Gresho, P. M., Lee, R. L., Sani, R. L., Maslanik, M. K., and Eaton, B. E., "The Consistent Galerkin FEM for Computing Derived Boundary Quantities in Thermal and/or Fluid Problems," *International Journal for Numerical Methods in Fluids*, Vol. 7, No. 4, 1987, pp. 371–394.

[6]Spalart, P. R., "Trends in Turbulence Treatments," AIAA Paper 2000-2306, Jan. 2000.

[7]Hellsten, A., and Laine, S., "Extension of the k–ω-SST Turbulence Model for Flows over Rough Surfaces," AIAA Paper 97-3577, Jan. 1997.

[8]Beaugendre, H., "A PDE-Based 3D Approach for In-Flight Ice Accretion," Ph.D. Dissertation, McGill Univ., Montreal, QC, Canada, June 2003.

[9]Blanchard, A., "Analyse Expérimentale et Théorique de la Structure de la Turbulence d'une Couche Limite sur Paroi Rugueuse," Ph.D. Dissertation, Unite d'Enseignement et de Recherche-Ecole Nationale Superieure de Mecanique et d'Aerotechnique, Univ. de Poitiers, Poitiers, France, May 1977.

[10]Aupoix, B., and Spalart, P. R., "Extensions of the Spalart–Allmaras Turbulence Model to Account for Wall Roughness," *International Journal of Heat and Fluid Flow*, Vol. 24, No. 4, Aug. 2003, pp. 454–462.

[11]Wright, W. B., and Rutkowski, A., "Validation Results for LEWICE 2.0," [CD-ROM], NASA CR-1999 203690, Jan. 1999.

Downloaded by PRINCETON UNIVERSITY on August 28, 2015 | http://arc.aiaa.org | DOI: 10.2514/2.7214

Benefit and Performance of Various Vortex Flap Configurations

Kenichi Rinoie*
University of Tokyo, Tokyo 113-8656, Japan

Introduction

THE leading-edge vortex flap (LEVF) is one of the devices that can improve the aerodynamic efficiency of delta wings at low speeds.[1] The LEVF is a full-span deflectable flap attached to the leading edge of the delta wing. With the flap deflected downward, a leading-edge separation vortex can be formed over the forward-facing flap surface. The vortex suction force acting normal to the flap surface generates a thrust component. Hence, this leading-edge suction reduces the drag of the wing and improves the lift/drag ratio at a given lift coefficient. Reference 2 contains an overview of LEVF research. Many tests have been done that confirm the benefit of the LEVF.[3,4] It has also been pointed out that LEVFs are effective for reduction of takeoff noise associated with the low-speed inefficiency of the delta wing used for the supersonic transport.[5]

It is clear that the vortex flap deflection angle is an important factor that determines the formation of the leading-edge separation vortex on the flap surface and the improvements of the lift/drag ratio of the delta wing. There are other factors that affect the vortex flap characteristics: 1) sweepback angle, 2) area ratio of the LEVFs/the delta wing, and 3) leading-edge shapes, that is, sharp or rounded leading edges. The sweepback angle determines the original delta wing aerodynamic characteristics, and hence, the performance of the LEVFs will also be affected. The area of the vortex flaps also affects the formation of the leading-edge separation vortex on the flap surface. As for leading-edge shapes, by deflecting the rounded LEVF, suction forces, which are caused both by the leading-edge separation vortex over the flap surface and by the rounded leading edge, may reduce the drag component and increase the lift/drag ratio.

Several experimental studies have been conducted using delta wing models with tapered vortex flaps that have different sweepback angles,[6–8] different flap areas,[9] and different leading-edge shapes.[10] The aim of this note is to discuss and summarize the benefit of vortex flaps that have different configurations, by reviewing the experimental results obtained by the author and others.

Experimental Details

The plan shape of the vortex flap is mainly classified into two different types. First is the flap that has a constant chord length along the whole part of the wing span. Many studies have investigated this type of vortex flap.[1,11] Another type is a tapered vortex flap. Figure 1 shows a schematic diagram of the tapered vortex flaps. The delta wing has vortex flap hinge lines running from the wing apex to the trailing edge. The vortex flap deflection angle δ_f is defined as the angle measured in the plane normal to the hinge line. The flap hinge-line position fr is defined as

$$fr = h/(b/2) \tag{1}$$

Received 21 July 2003; accepted for publication 25 July 2003. Copyright © 2003 by the American Institute of Aeronautics and Astronautics, Inc. All rights reserved. Copies of this paper may be made for personal or internal use, on condition that the copier pay the $10.00 per-copy fee to the Copyright Clearance Center, Inc., 222 Rosewood Drive, Danvers, MA 01923; include the code 0021-8669/03 $10.00 in correspondence with the CCC.

*Associate Professor, Department of Aeronautics and Astronautics, 7-3-1 Hongo, Bunkyo-ku. Senior Member AIAA.